Pergamon

Geochimica et Cosmochimica Acta, Vol. 60, No. 9, pp. 1615–1631, 1996

0016-7037/96 $15.00 + .00

PII S0016-7037(96)00031-2

# Core crystallization and silicate-metal mixing in the parent body of the IVA iron and stony-iron meteorites

EDWARD R. D. SCOTT, HENNING HAACK,* and TIMOTHY J. MCCOY†

Hawai'i Institute of Geophysics and Planetology, School of Ocean and Earth Science and Technology, University of Hawai'i at Manoa, Honolulu, HI 96822, USA

(*Received October* 14, 1994; *accepted in revised form January* 10, 1996)

**Abstract**—We have analyzed metallic and silicate phases in the IVA iron meteorites and two related stony irons, Steinbach and São João Nepomuceno. Analyses of bulk metal phases in the two stony irons using INAA show that they plot as close to the chemical trends within group IVA as most IVA irons, indicating a common source. Our fractional crystallization models for the IVA chemical trends suggest that the irons crystallized from a metallic melt that initially contained 2.5 ± 1 wt% S. After S concentrations in the liquid reached 6 wt%, liquid trapping during crystallization increased the apparent distribution coefficient for S, as in group IIIAB. Compositions of the metal fractions in Steinbach and São João Nepomuceno match the calculated solid compositions after 50 ± 10% and 80 ± 10%, respectively, of the metallic melt had crystallized. We confidently conclude that the IVA irons and metal in the two stony irons were derived from the core of a single asteroid that fractionally crystallized. The wide range of metallographic cooling rates of IVA irons cannot result from crystallization in isolated pools in one or more bodies, as some authors have argued. Large depletions of Ga, Ge, and other moderately volatile elements in group IVA are unlikely to result from planetary processes; they may have been inherited from chondritic precursor material.

The two IVA stony irons contain up to 60 vol% of a unique, coarse-grained mixture of tridymite, orthobronzite, and clinobronzite. Silicate-metal textures resemble those in rounded-olivine pallasites; both may result from the depression of cumulate silicates into underlying molten S-rich metal. Two IVA irons contain rare plate-like, silica crystals up to 10 mm long, but these occurrences seem unrelated to the stony-iron silicates. Because of the difficulty in forming the stony irons in an isolated, slowly cooling asteroid, we infer that they may have formed during the breakup and reassembly event invoked by Haack et al. (1995) to account for the fast cooling of Steinbach from 1200°C.

## 1. INTRODUCTION

Group IVA iron meteorites have most but not all of the chemical and mineralogical characteristics of iron meteorite groups such as group IIIAB that are generally believed to have formed in molten cores in asteroids (Schaudy et al., 1972; Wasson et al., 1989; Haack and Scott, 1993). IIIAB-like irons are different from the silicate-bearing IAB and IIICD irons, which are believed to have formed in impact-melt pools (Choi et al., 1995) or in S-rich cores (McCoy et al., 1993). Over fifty irons have been classified as IVA members (Appendix, Table A1) making this the fourth largest group of irons. The Ni-rich IVB irons have Ga concentrations that are 10× lower than those in group IVA and must have formed in an entirely different body (Wasson, 1974).

Despite the unusually low concentrations of Ga, Ge, and other moderately volatile siderophiles in the IVA irons, chemical trends within the group are broadly consistent with fractional crystallization of a metallic core (Willis and Goldstein, 1982; Jones and Drake, 1983). But this interpretation was questioned by Moren and Goldstein (1978, 1979), who found a wide variation in the metallographic cooling rates of IVA irons and an inverse correlation between cooling rate and bulk Ni concentration. They inferred that IVA irons formed in many separate metallic pools at various depths because core samples should have indistinguishable cooling rates. Willis and Wasson (1978a,b) tried to argue that the correlation between cooling rate and bulk Ni and the wide variation in cooling rates result from errors in the diffusion rates or phase diagram and that IVA irons cooled in a core. However, Rasmussen (1982) confirmed the wide range and inverse correlation found by Moren and Goldstein (1979). He suggested that low-Ni IVA irons come from pools in one body and that high-Ni IVA irons come from a second body, implying that the continuity of the chemical trends was fortuitous. Revised cooling rates for IVA irons are reported by Rasmussen et al. (1995).

Two stony-iron meteorites, Steinbach and São João Nepomuceno, which have abundant rounded pyroxene-tridymite inclusions (Reid et al., 1974; Bild, 1976; Prinz et al., 1984), have a fine octahedral Widmanstätten pattern and concentrations of Ni, Ga, Ge, and Ir in their metal that are very similar to those of group IVA irons (Schaudy et al., 1972; Kracher et al., 1980). Since density differences ensure that silicates will quickly rise through molten metal, it is difficult to understand their presence in meteorites that may be derived from an asteroidal core. Silicates have also been found in two

* *Present address:* Fysisk Institut, Odense Universitet, Odense, DK 5230, Denmark.
† *Present address:* Code SN4, NASA Johnson Space Center, Houston, TX 77058, USA.

Table 1. Concentrations of six elements in four IVA irons and the metal phases of two stony-irons, Steinbach and São João Nepomuceno.

| | Co mg/g | Cr µg/g | As µg/g | Au µg/g | Re µg/g | Ir µg/g |
|---|---|---|---|---|---|---|
| Hill City | 4.1 | 27† | 10.4 | 2.37 | 0.13† | 0.92 |
| Jamestown* | 3.4 | 500 | 1.8 | 0.56 | 0.28 | 3.2 |
| Rembang | 4.0 | 67 | 9.0 | 1.91 | 0.11 | 1.14 |
| São João Nepomuceno | 4.0 | 25 | 4.6 | 1.17 | 0.34 | 2.6 |
| Seneca Township | 4.0 | 60† | 6.0 | 1.56 | 0.14 | 1.63 |
| Steinbach | 4.2 | 50 | 12.7 | 2.94 | <0.07 | 0.86 |

* Only one sample analyzed; error is about 1.5x the normal value.
† Estimated error is twice the usual value.

IVA irons, Bishop Canyon and Gibeon; both contain large but very rare grains of $SiO_2$ (Schaudy et al., 1972; Buchwald, 1975). The oxygen isotopic composition of the silicates in São João Nepomuceno, Steinbach, and Gibeon are unlike those in any other meteorites, except for those in L and LL chondrites (Clayton et al., 1983). However, it is rather unlikely that there was extensive melting in the L and LL parent bodies, as differentiated silicates have not been identified despite thorough impact mixing and sampling of their parent bodies (Taylor et al., 1987).

Silicates in Steinbach are also anomalous because they appear to have been quenched from high temperature (Reid et al., 1974). This conclusion, which has been confirmed by Haack et al. (1995), has not generally been considered in discussions of the thermal history and origins of IVA irons. This may be because the association of Steinbach with IVA irons was questioned, or because the proposed quenching history did not seem plausible. Prinz et al. (1984) have briefly discussed possible origins for the Steinbach and São João Nepomuceno silicates.

We have attempted to elucidate the origin and evolution of group IVA irons and stony-irons using three approaches. (1) Metal portions of Steinbach and São João Nepomuceno and four IVA irons have been analyzed using instrumental neutron activation analysis. Published compositional data for IVA irons have been compiled to test how closely the metal compositions of the stony irons match those of the group IVA irons. (2) The chemical trends in group IVA have been investigated using the fractional crystallization models of Haack and Scott (1993) to better understand their origin. (3) Silicates in the two IVA-like stony irons and rare silica grains in two IVA irons have been analyzed using electron-probe analysis to learn more about the origin of the silicates. We conclude that the IVA irons, like the IIIAB irons, did form in a core and that the two stony irons are not mere mineralogical curiosities but provide important constraints on the formation and evolution of the IVA core.

## 2. TECHNIQUES AND SAMPLES

Samples weighing 0.5–1 g of four iron meteorites and metal from two stony irons were analyzed by instrumental neutron activation analysis at UCLA using the procedures described by Scott (1978a). The sources and catalog numbers for these samples are given by Scott (1978b), who also gives W concentrations for these irons. The data given in Table 1 are means of duplicate analyses except where noted. The 95% confidence limits of the means in Table 1 are 8% for Au and Ir, 7% for As and Co, 15% for Re, and 23% for Cr (Scott, 1978a).

Eight polished thin sections of Steinbach were prepared from material and covered sections from the Bergakademie Freiberg (University of Hawaii section # 209-214, 231, 232P). Three polished thin sections of São João Nepomuceno and one other Steinbach section (USNM 496) were loaned by the Smithsonian Institution. A polished end piece of Bishop Canyon (Arizona State University sample no. 360.1), which contains silica grains (Buchwald, 1975), was cut perpendicular to the original face across the two large silica grains. A polished slice of Gibeon containing a large silica lath that was originally described by Schaudy et al. (1972) and is owned by J. T. Wasson, was loaned to us by K. L. Rasmussen.

Petrography and modal analyses were performed in reflected and transmitted light using a Nikon Microphot polarizing microscope. Pyroxene compositions were analyzed using a Cameca Camebax electron microprobe operated at 15 keV accelerating voltage, 15 nA beam current, and a fully focused beam. Analyses of tridymite were made on a Cameca SX-50 electron microprobe using a 15 keV accelerating voltage, 10 nA beam current, and a 10 $\mu$m beam. Counting times for $Al_2O_3$ were 60 s each on peak and background. Count times of 30 s were used for other elements. Data were corrected using the PAP ZAF program.

## 3. RESULTS

### 3.1. Metal Composition

In Table 1 we report instrumental neutron activation analyses of metal in the two IVA-like stony irons, Steinbach and São João Nepomuceno. For Steinbach, there are some discrepancies between our data and literature data. Schaudy et al. (1972) reported 0.053 $\mu$g/g Ir. This value should have been 0.53 $\mu$g/g (Wasson, 1974), but it is still lower than our value of 0.86 $\mu$g/g. Our values for Ir, As, and Au in Steinbach are also higher than those of Ryan et al. (1990), conceivably because of silicate contamination in the latter. Because our replicates agree, we prefer our values. The analyses of the four IVA irons listed in Table 1 are consistent with published data for other IVA irons. We have used analyses from Table 1 and literature data (see Appendix) to compile a database for the concentrations of eleven elements in the IVA irons. In Fig. 1 we show element-Ni plots for Au, As, Ga, Ge, Ir, Re, W, and Cr.

#### *3.1.1. Classification of group IVA outliers*

On element-Ni plots, the IVA members that show the largest scatter are the three high-Ni irons (Fig. 1). Because they are critical in establishing the chemical trends in IVA and testing crystallization models, we reassess their classification. Two of these irons, Chinautla and Duel Hill (1854), were classified by Schaudy et al. (1972) as anomalous IVA members; the latter was reclassified as IVA by Malvin et al. (1984), partly because they discovered an error in the Ir analysis of Schaudy et al. (1972). The third, Fuzzy Creek with 11.8% Ni, was identified by Malvin et al. (1984) as the highest-Ni IVA member. We conclude that these three irons are all bona fide IVA members and note that the increased scatter with increasing Ni is analogous to that in group IIIAB (Haack and Scott, 1993). These three irons

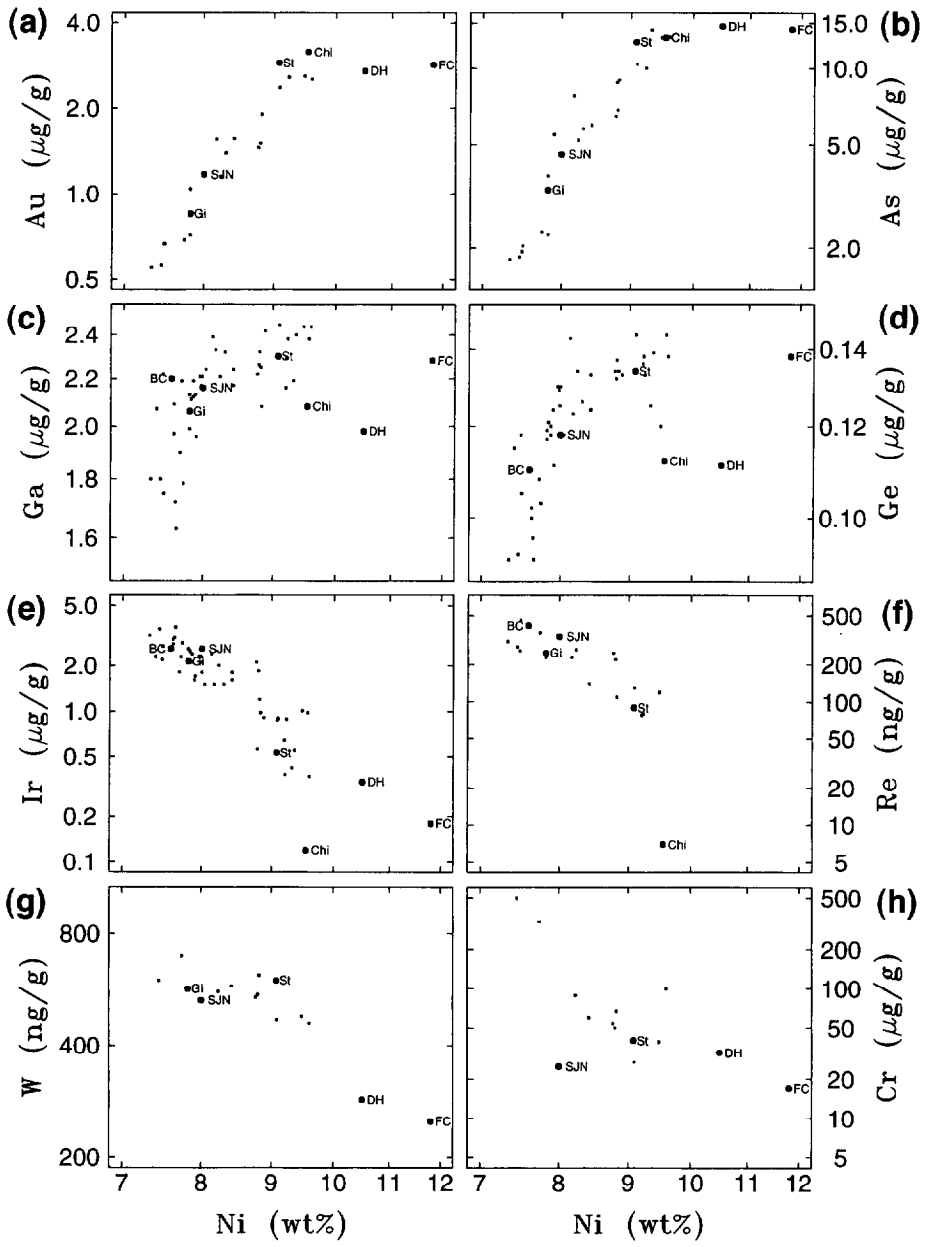


FIG. 1. Logarithmic plots of (a) Au, (b) As, (c) Ga, (d) Ge, (e) Ir, (f) Re, (g) W, and (h) Cr against Ni for group IVA meteorites. The four silicate-bearing meteorites are labeled: Bishop Canyon (BC), Gibeon (Gi), São João Nepomuceno (SJN), and Steinbach (St). The three high-Ni IVA irons meteorites, which are discussed in the text, are: Chinautla (Chi), Duel Hill (1854) (DH), and Fuzzy Creek (FC). Data from sources listed in Table A1.

also cause the Au-Ni and As-Ni trends to flatten with increasing Ni (Fig. 1).

Malvin et al. (1984) noted that Cu concentrations in Fuzzy Creek and Duel Hill are about 2× higher than predicted from an extrapolation of the negative Cu-Ni trend shown by IVA irons with <96 mg/g Ni. They suggested that the reversal in the Cu-Ni trend was due to anomalous addition of a liquid rich in FeS and Cu during the crystallization of these irons. However, we believe a more plausible explanation is a rapid decrease in the Cu distribution coefficient with increasing S concentration in the liquid. Sellamuthu and Goldstein (1985) observed such a decrease in their dynamic experiments.

To search for other irons that may be related to group IVA, we have plotted in Fig. 2 the compositions of group IVA irons and ungrouped irons with 0.5–5 μg/g Ga and 0.03–0.3 μg/g Ge. Dermbach, which has 42% Ni, and EET 87516, which has a Ga concentration in the IVA range but has not been analyzed for Ge (Wasson, 1990), do not appear to be related to group IVA. Only four other ungrouped irons have Ga and Ge concentrations in the ranges shown in Fig.

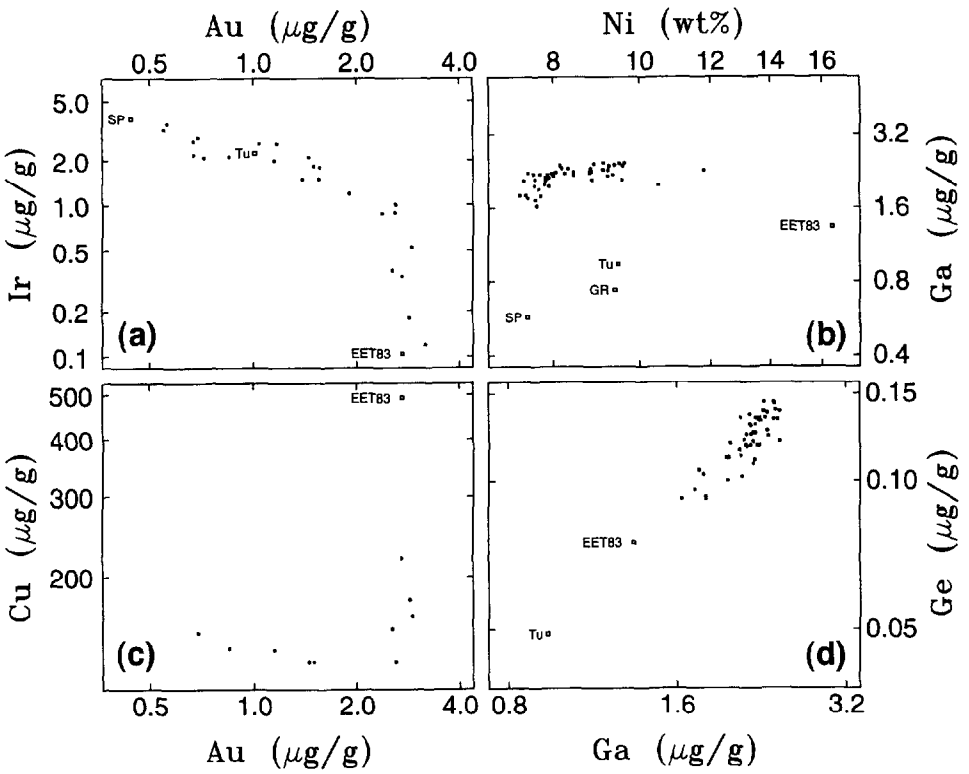


FIG. 2. Logarithmic plots of (a) Ir vs. Au, (b) Ga vs. Ni, (c) Cu vs. Au, and (d) Ge vs. Ga for iron meteorites in group IVA and some ungrouped iron meteorites with compositions close to those of group IVA iron meteorites: EET83: EET 83230; Tu: Tucson; GR: Glen Rose; SP: Santiago Papasquiero. EET 83230, unlike the others, appears to be closely related to group IVA and may be a high-Ni member.

2. This is many times less than the number with Ga and Ge concentrations near group IIIAB values.

Of the irons currently classed as ungrouped that are plotted in Fig. 2, Tucson, Glen Rose, and Santiago Papasquiero lie far from the IVA field on the Ga-Ni plot (Fig. 2b) and are clearly unrelated to group IVA. However, EET 83230, which has been analyzed for fifteen elements by Wasson et al. (1989) and Jarosewich (1990), shows a remarkable chemical affinity for group IVA, despite a Ni concentration of 16.3%. On interelement plots, EET 83230 matches fairly well extrapolations of the chemical trends defined by the high-Ni IVA irons, including those discussed above. On Ga-Ni, Ge-Ni, and P-Ni plots, the high-Ni trends are not well-defined, but for Ga-Ge, Ir-Au, and Cu-Au (Fig. 2) and on plots of Au, As, Ir, W, Co, and Cr against Ni (Fig. 2 of Malvin et al. (1984) and our Fig. 1), we find strong evidence for a link between EET 83230 and group IVA. The low background of ungrouped irons in Fig. 2 enhances this belief. The major reason for doubting that EET 83230 is a IVA member is the uncertainty in the large extrapolation of group IVA to higher Ni concentrations. In our fractional crystallization modeling of IVA trends, we were unable to generate fractionation trends that extend to the composition of EET 83230. But this may not be a valid reason for doubting the relationship with IVA as we also failed to satisfactorily model the compositions of Duel Hill (1854) and Fuzzy Creek. In the Appendix (Table A2), we tentatively list EET 83230 as a IVA iron.

*3.1.2. Siderophile element trends in IVA irons*

The chemical trends defined by group IVA iron meteorites in Figs. 1 and 2 are in general similar to the trends defined by group IIIAB, the largest group of iron meteorites (Haack and Scott, 1993). Some differences may, however, be important in understanding the formation of these two large groups of iron meteorites. On the Au-Ni and As-Ni plots, group IIIAB trends are linear, but IVA trends are markedly curved and level off at high Ni concentrations.

With the addition of the high-Ni IVA irons discussed above, group IVA shows reversals in the Ga-Ni and Ge-Ni trends that are analogous to those in group IIIAB. The banana-shaped Ni vs. Ga and Ge trends observed in IVA are rotated counterclockwise relative to the corresponding trends in IIIAB. This difference is probably part of a general trend from S-rich IIAB, which shows predominantly negative Ga and Ge-Ni trends, to S-poor group IVB, which shows positive correlations. The increases of $K_{Ga}$ and $K_{Ge}$ with S (Jones and Malvin, 1990; Haack and Scott, 1993) probably account for these changes. The negative slope of the Ni-Ir trends in these groups also decreases from IIAB to IVB (Scott, 1972).

The near-vertical Ga-Ni and Ge-Ni trends observed in low-Ni group IVA irons in Fig. 1 seem to require that the solid crystallizing from the IVA core did not change its Ni concentration during the first phase of the crystallization process. This is enigmatic since $K_{Ni}$ initially is less than unity and is expected to increase as S increases in the liquid during crystallization.

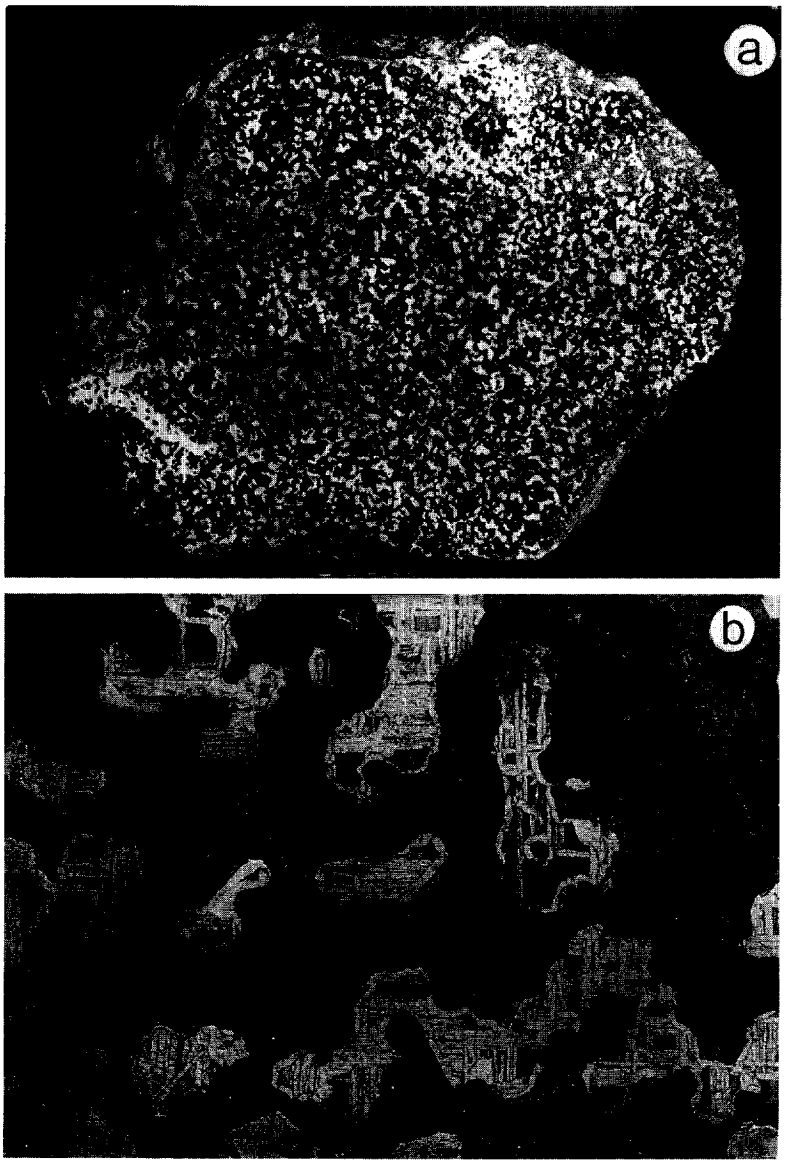


FIG. 3. Photographs of the Steinbach stony-iron meteorite. (a) A polished slice showing ~30 vol% white grains of metallic Fe,Ni and troilite in a dark silicate matrix. Most metallic grains are uniformly distributed with apparent widths of 1–10 mm although two larger metal-rich areas are present. Longest dimension: 51 cm. (b) Part of an etched slice showing fine, oriented kamacite lamellae in metallic Fe,Ni grains that are rimmed by kamacite. The continuity of the Widmanstatten pattern across the field shows that the grains are connected and once formed a single large skeletal taenite crystal. Width: 34 mm. (Photos from Dr. Hans-Joachim Blankenburg.)

### *3.1.3. Metal in IVA stony irons*

On most interelement plots, the compositions of the metallic portions of the two stony irons, Steinbach and São João Nepomuceno, are indistinguishable from those of the IVA irons (Fig. 1). The Au and As concentrations in Steinbach seem somewhat high, and Cr in São João Nepomuceno is rather low. But overall, they appear to plot as close to the IVA trends as most IVA irons.

J. T. Wasson (pers. commun., 1995) has analyzed new samples of Steinbach metal and finds a higher Ni concentration than Schaudy et al. (1972) reported (10.0 vs. 9.1%) and a lower Au concentration than we list (2.5 vs. 2.9 $\mu$g/g). These small differences, which may result from problems with silicate contamination or sample heterogeneity, shift Steinbach to the high-Ni edge of the IVA field on some plots but do not affect our basic conclusions.

## 3.2. Mineralogy of Silicate-bearing IVA Meteorites

### *3.2.1. Steinbach*

The unusual metal-silicate texture of Steinbach is shown in Fig. 3a, a photo of the largest specimen, which is at the Bergakademie Freiberg (Hoppe, 1975; Rösler et al., 1978). Metal and troilite, which cannot be distinguished from each


FIG. 4. Photomicrographs of the Steinbach meteorite. (a) Reflected-light photomicrograph showing pyroxene (Fs 15) between Fe,Ni metal (m) and tridymite (si). Troilite (t) occurs as large interstitial grains and tiny blebs in pyroxene. Tridymite (si) contains a circular inclusion of pyroxene. (b) Transmitted light photomicrograph in crossed polars showing tridymite (si) partly surrounding and embaying two interlocking orthobronzite (o) crystals; the smaller, darker one in the center contains patches of twinned clinobronzite. Scale bars: 50 $\mu$m.

other in this photo, occupy 29 vol% as irregularly shaped grains. Except in two small, metal-rich areas, metallic grains are fairly uniformly distributed, generally have apparent sizes of 1–20 mm, and typically appear to be enclosed by silicate. However, etching of the metal shows that the Widmanstätten pattern is uniformly oriented over distances of at least several cm (Fig. 3b). Plate 31 of McCall (1973) shows a 96 mm wide slice, which also has a single Widmanstätten orientation. Thus, the metal grains in Steinbach form a network in which taenite crystals can exceed 10 cm in length. A mixture of pyroxene and $SiO_2$ fills the spaces within this network with apparent grain sizes of 1–4 mm.

In thin section, metal-silicate and silicate-silicate grain boundaries are typically complex, not straight. Metal-silicate boundaries are scalloped (Fig. 4a): metallic cusps mark existing and presumably, preexisting, silicate grain boundaries and fractures. Troilite forms partial rims on some metal grains and grains between silicates. In addition, most pyroxenes contain tiny inclusions of troilite and more rarely, metal, that may be rounded or irregular in shape (Fig. 4b). Pyroxenes and $SiO_2$ are intergrown as if they co-crystallized (Fig. 4b).

Reid et al. (1974) and Dollase (1967) identified the silicates as orthobronzite, clinobronzite, and tridymite; we did not identify any others. Abundant orthopyroxene typically exhibits sharp extinction. Twinned clinobronzite occurs as

Table 2. Modal analyses (vol.%) of thin sections of Steinbach.

| Mineral | USNM 496 | UH 232P | UH 209 | UH 210 | UH 211 | UH 212 | UH 213 | UH 214 | UH 231 | Average[5] |
|---|---|---|---|---|---|---|---|---|---|---|
| Fe,Ni Metal | 37.2 | 38.2 | 18.0 | 70.0 | 21.6 | 49.7 | 47.8 | 42.7 | 3.0 | 32.2 |
| Troilite | 0.8 | 5.6 | 8.2 | 0.8 | 8.9 | 1.2 | 4.3 | 1.7 | 18.9 | 6.6 |
| FeOOH[1] | 2.9 | 0.0 | 0.7 | 0.1 | 0.5 | 0.0 | 0.7 | 0.4 | 0.1 | 0.6 |
| Orthobronzite | 45.8 | 42.3[4] | 41.5 | 16.6 | 39.8 | 31.3 | 34.2 | 36.7 | 49.1 | 38.0 |
| Clinobronzite[2] | 1.0 | -- | 3.6 | 0.0 | 1.2 | 0.0 | 0.3 | 0.8 | 2.2 | 1.6 |
| Tridymite | 11.8 | 13.8 | 27.7 | 12.4 | 27.7 | 17.6 | 12.3 | 17.5 | 26.4 | 20.8 |
| Chromite | 0.1 | 0.0 | 0.0 | 0.0 | 0.0 | 0.0 | 0.0 | 0.0 | 0.0 | 0.0 |
| # of Counts | 1483 | 978 | 1164 | 740 | 559 | 249 | 251 | 234 | 1291 | |
| Area ($mm^2$) | 150.5 | 219 | 540.5 | 245 | 213 | 88 | 88 | 76 | 174 | 1794 |
| Metal/Silicate[3] | 0.7 | 0.8 | 0.4 | 2.4 | 0.5 | 1.0 | 1.1 | 0.8 | 0.3 | 0.7 |
| Px/Trid | 4.0 | 3.1 | 1.6 | 1.3 | 1.5 | 1.8 | 2.8 | 2.1 | 1.9 | 1.9 |

[1] Hydrated iron oxides of terrestrial origin.
[2] Striated low-Ca pyroxene.
[3] Ratio: (Fe,Ni+Troilite+FeOOH) / (Opx+Cpx+Trid)
[4] Opx and Cpx could not be distinguished.
[5] Weighted Average; Individual sections weighted by section area.

islands inside large orthopyroxene crystals and occasionally along pyroxene-$SiO_2$ contacts. In some instances, clinobronzite islands in different orthopyroxenes several millimeters apart have uniform orientations. Modal analyses of nine Steinbach thin sections having a combined area of 18 $cm^2$ are shown in Table 2. Overall, metal and troilite (and their weathering products) occupy 39 vol%, c.f. 29% from Fig. 3a. Chromite, though present in most thin sections, occupies <0.1%. The pyroxene/tridymite ratio varies from 1.3 to 4 in the nine sections analyzed, consistent with the large grain sizes. Our mean value of 1.9 for the pyroxene/tridymite ratio is somewhat higher than that of Prinz et al. (1984) who found a ratio of 1.3. Twinned clinopyroxene is highly variable in abundance in thin sections, ranging from 0 to 3.6 vol%.

We have analyzed orthopyroxene, low-Ca clinopyroxene and tridymite in Steinbach (Table 3). Our analyses of ortho- and clinobronzite agree well with those of Reid et al. (1974). We confirm that the mean composition of orthopyroxene grains is higher in Ca and Fe and lower in Mg than the clinopyroxene mean, although these differences are well within the $1\sigma$ variations of individual analyses. Differences in the FeO concentrations are consistent with derivation by quenching of clinopyroxene from protopyroxene that equilibrated with orthopyroxene at 1200°C (Reid et al., 1974). Tridymite contains 0.1–0.2% $Al_2O_3$, FeO, and $Na_2O$.

### 3.2.2. *São João Nepomuceno*

The whole São João Nepomuceno meteorite including several complete slices is located at the Smithsonian Institution. Very brief descriptions have been published by Bild (1976, 1977) and Prinz et al. (1984) who found that the major silicates were tridymite, orthobronzite, and clinobronzite, as in Steinbach.

Silicates comprise 19 vol% of the surface area of a 20 × 10 cm slice but they are distributed very heterogeneously. Figure 5 shows a silicate-rich portion of this slice; the largest silicate-free area is 10 × 20 cm. At least six different parent taenite crystals are visible in this slice; the largest is 4 × 8 cm. Silicates are partly concentrated on the taenite grain boundaries. Silicate-rich regions show metal-silicate intergrowths that resemble those in Steinbach.

The three thin sections of São João Nepomuceno that we studied, which are all from silicate-rich regions, show silicate textures that are very similar to those in Steinbach except for the extensive terrestrial weathering in two sections of São João Nepomuceno. Modal analysis shows that, as in Steinbach, orthobronzite is much more abundant than clinobronzite (Table 4). Tridymite, and possibly also clinobronzite, constitutes a smaller fraction of the silicates in São João Nepomuceno than in Steinbach.

Orthobronzite is slightly poorer in FeO than in Steinbach; Fs 14.2 ± 0.2 cf. Fs 15.0 ± 0.5 in Steinbach (Table 3). As in Steinbach, the mean composition of orthobronzite is marginally higher in Ca, Fe, and Al and lower in Mg than the mean composition of clinobronzite, although the differences are within the $1\sigma$ variation of individual analyses. Tridymite contains concentrations of $Al_2O_3$, FeO, and $Na_2O$ (0.2–0.3%) that are slightly higher than those in Steinbach.

### 3.2.3. *Bishop Canyon*

Silica was reported in a single specimen of Bishop Canyon (ASU no. 360.1): two silica grains were identified by Buchwald (1975). For our study, the sample was cut perpendicular to the plane of the original surface to allow more detailed petrographic descriptions and chemical analyses. This shows that the two grains are plate-like grains with maximum dimensions of 10 and 5 mm (Fig. 6). Troilite with exsolved daubreelite occurs around the grains. The silica is probably tridymite, as noted by Buchwald (1975). Concentrations of Na and Al are lower than in the two IVA stony irons, but the FeO concentration of 0.4 ± 0.3 is higher (Table 3). Analyses of thirteen points in the silica grains revealed no systematic zoning.

Table 3. Silicate compositions (wt. %) in IVA iron meteorites.

| Meteorite | Mineral | $SiO_2$ | $TiO_2$ | $Al_2O_3$ | $Cr_2O_3$ | FeO | MnO | MgO | CaO | $Na_2O$ | Total | N | Fs |
|---|---|---|---|---|---|---|---|---|---|---|---|---|---|
| Steinbach | Opx | 56.1 | <0.03 | 0.25 | 0.58 | 9.86 | 0.53 | 31.1 | 0.31 | <0.03 | 98.73 | 6 | 15.0 |
| | | *0.33* | | *0.14* | *0.19* | *0.32* | *0.01* | *0.38* | *0.13* | | | | *0.5* |
| | Cpx | 56.2 | <0.03 | 0.22 | 0.49 | 9.50 | 0.49 | 31.5 | 0.14 | <0.03 | 98.54 | 6 | 14.5 |
| | | *0.38* | | *0.03* | *0.05* | *0.28* | *0.04* | *0.25* | *0.08* | | | | *0.5* |
| | $SiO_2$ | 99.6 | n.d. | 0.23 | n.d. | 0.08 | n.d. | <0.03 | <0.03 | 0.13 | 100.04 | 10 | |
| | | *0.24* | | *0.05* | | *0.05* | | | | *0.03* | | | |
| São João Nepomuceno | Opx | 55.9 | <0.03 | 0.28 | 0.74 | 9.30 | 0.59 | 31.2 | 0.45 | <0.03 | 98.46 | 3 | 14.2 |
| | | *0.11* | | *0.07* | *0.11* | *0.08* | *0.05* | *0.31* | *0.18* | | | | *0.2* |
| | Cpx | 56.1 | <0.03 | 0.22 | 0.53 | 8.97 | 0.53 | 31.8 | 0.12 | <0.03 | 98.27 | 2 | 13.6 |
| | | *0.16* | | *0.01* | *0.12* | *0.00* | *0.02* | *0.06* | *0.01* | | | | *0.0* |
| | $SiO_2$ | 99.6 | n.d. | 0.31 | n.d. | 0.20 | n.d. | <0.03 | <0.03 | 0.18 | 100.29 | 10 | |
| | | *0.20* | | *0.02* | | *0.20* | | | | *0.02* | | | |
| Gibeon | $SiO_2$ | 99.6 | n.d. | 0.04 | n.d. | 0.36 | n.d. | <0.03 | <0.03 | <0.03 | 100.00 | 10 | |
| | | *0.47* | | *0.03* | | *0.13* | | | | | | | |
| Bishop Canyon | $SiO_2$ | 100.0 | n.d. | 0.02 | n.d. | 0.39 | n.d. | <0.03 | <0.03 | <0.03 | 100.41 | 13 | |
| | | *0.42* | | *0.01* | | *0.29* | | | | | | | |

Italicized figures are 1σ of compositional variability of the N analyses.
n.d. = not determined

### 3.2.4. *Gibeon*

Although Gibeon is one of the most widely distributed iron meteorites, silicates are very rare (Buchwald, 1975). Schaudy et al. (1972) described a specimen in which tridymite formed intersecting veins 1 mm wide and more than 25 mm long. They inferred that enstatite platelets reported in another Gibeon sample were actually tridymite also. We report some new observations and chemical data from the Schaudy et al. (1972) sample: further details are given by Ulff-Møller et al. (1995).

We observed three silica grains, 9 by 1 mm, 6 by 1 mm, and 6 mm by 600 μm, which appear to be fragments of a single plate-like crystal. The first two grains are aligned but the third appears to be misoriented by 10°. We infer that the silica crystal was originally at least 21 mm long, and that

FIG. 5. Part of a polished and etched slice of the São João Nepomuceno IVA stony-iron meteorite showing silicates heterogeneously distributed in Fe,Ni metal having a fine octahedral Widmanstätten pattern. The silicate-rich region in the upper half resembles Steinbach (Fig. 3). The silicate mineralogy (orthobronzite, tridymite, clinobronzite) and metal compositions are also very similar. Scale bar: 2 cm; Smithsonian Institution photo.

Table 4. Modal analyses (vol.%) of three São João Nepomuceno thin sections.

| Mineral | 1 | 2 | 3 | Average[4] |
|---|---|---|---|---|
| Fe,Ni Metal | 39.6 | 0.1 | 62.1 | 44.1 |
| Troilite | 1.6 | 1.9 | 7.2 | 4.6 |
| FeOOH[1] | 6.4 | 31.8 | 0.9 | 8.3 |
| Orthobronzite | 46.7 | 63.8 | 23.7 | 37.8 |
| Clinobronzite[2] | 0.0 | 0.2 | 0.0 | 0.1 |
| Tridymite | 5.6 | 1.7 | 6.0 | 5.1 |
| Chromite | 0.0 | 0.1 | 0.1 | 0.1 |
| # of Counts | 2000 | 836 | 4345 | |
| Area ($mm^2$) | 103.5 | 68.5 | 192 | 364 |
| Metal/Silicate[3] | 0.9 | 0.5 | 2.4 | 1.3 |
| Px/Trid | 8.3 | 37.6 | 4.0 | 7.4 |

[1] Hydrated iron oxides of terrestrial origin.
[2] Striated low-Ca pyroxene.
[3] Ratio: (Fe,Ni+Troilite+FeOOH) / (Opx+Cpx+Trid)
[4] Weighted Average; Individual sections weighted by section area.
All three section are un-numbered and labelled as follows: 1, "Nepo-1"; 2, "Nepo-2"; 3, "USNM".

it was broken before the formation of the Widmanstatten pattern.

The Gibeon tridymite crystal contains <0.03 wt% MgO, CaO, and $Na_2O$, as in the Bishop Canyon tridymite (Table 3). Mean FeO and $Al_2O_3$ concentrations are also comparable in the two occurrences, but the Gibeon crystal is systematically zoned: FeO concentrations increase from 0.1 wt% in the core to 0.2 wt% in the rim while $Al_2O_3$ decreases from 0.09 to 0.02 wt% (Fig. 7).

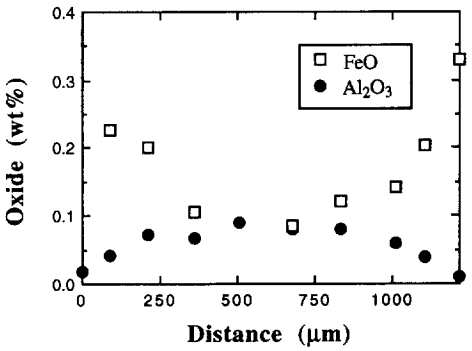


FIG. 7. Zoning profiles across an $SiO_2$ grain in the Gibeon IVA iron: $Al_2O_3$ concentrations decrease from core to rim, whereas FeO concentrations increase.

## 4. DISCUSSION

### 4.1. Fractional Crystallization Models for IVA Metal

#### *4.1.1. Distribution coefficients and models*

We have modeled the compositional trends defined by the group IVA iron meteorites using a simple one-dimensional fractional crystallization model (Haack and Scott, 1993). The solid metal/liquid metal distribution coefficients ($K$)

FIG. 6. Sample of Bishop Canyon, a IVA iron meteorite, that contains rare silica. Two dark, plate-like grains are visible at the bottom of the nearly perpendicular faces. Arizona State University specimen 360.1: length of straight edge is 3.2 cm.

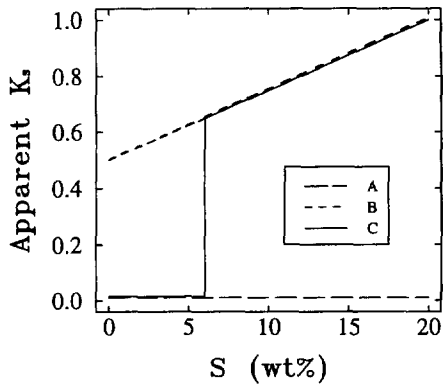


FIG. 8. Apparent distribution coefficient for S ($K_S$) against S concentration in the liquid for the three closed-system, fractional crystallization models. Model A uses an equilibrium value of 0.01 for $K_S$. Model B uses an empirical relationship for $K_S$ derived from group IIIAB data (Haack and Scott, 1993). Model C uses an equilibrium value of 0.01 for liquids with <6% S, and the model B relationship for liquids with >6% S.

and their dependence on S and P concentrations are based on the formulations of Jones and Malvin (1990). Coefficients for Ga and Co in the S-free system were modified as described in Haack and Scott (1993). We have investigated a range of models to study the effects of (1) different initial S concentrations in the liquid, (2) trapping of S-rich liquid during crystallization, and (3) assimilation or addition of liquid during crystallization. We present the results of four models which best illustrate the effects of these parameters. In all four, after each crystallization step the liquid was assumed to be completely mixed. This is a necessary, although only approximately correct, assumption in this type of simple one-dimensional model. Initial liquid compositions were treated as free parameters.

The three closed-system models (A–C) differ chiefly in their distribution coefficients for S and their dependence on the S concentration in the liquid. Prior to the work of Haack and Scott (1993), fractional crystallization models for iron meteorites used $K_S \approx 0$, since the equilibrium solubility of S in solid metal is very close to zero (Willis and Goldstein, 1982). For our equilibrium model (model A), we used $K_S = 0.01$. However, Haack and Scott (1993) argued that the presence of troilite nodules indicates much higher apparent values for $K_S$, which they attributed to the accumulation of S-rich liquid in structural traps formed by the advancing solid or at the top of the core. In our model B for group IVA, we have used the same dependence of apparent $K_S$ on S that Haack and Scott (1993) used to model the IIIAB trends (Fig. 8).

If liquid trapping was aided by the formation of immiscible S-rich liquids in the boundary layer, as Kracher et al. (1977) and Haack and Scott (1993) believed, then we might expect that trapping of S could only take place above some threshold S and P concentration where formation of immiscible liquid is possible. The S concentration of IIIAB and IVA irons (Buchwald, 1975) and the fractional crystallization models of Jones and Drake (1983) and Sellamuthu and Goldstein (1985) suggest that the initial S concentration of the IVA liquid was indeed less than that in the IIIAB core. Thus, our third model (C) is a composite model: for liquids with <6% S (the initial S concentration in our preferred model for IIIAB) we use $K_S = 0.01$, as in model A, and for liquids with >6% S, $K_S$ increases continuously from 0.65, as in model B (Fig. 8). This is consistent with the observation that low-Ni IVA irons have less troilite than high-Ni IVA members (Buchwald, 1975). For simplicity, in models C and D we have used the same initial liquid composition that was chosen for model A (Table 5). For model B, we chose an initial liquid composition that would give the same trajectory on interelement plots as model C for liquids with >6% S.

Pernicka and Wasson (1987) and Malvin (1988) proposed that a primitive liquid with approximately chondritic ratios of siderophiles leaked into the core during crystallization. This would significantly increase the Ir concentration in the highly depleted residual liquid during the final stages of crystallization and thus increase the Ir concentration of the crystallizing solid. Haack and Scott (1993) argued that it was not possible to supply the core with molten metal during crystallization since the base of the mantle and the top of the core were almost entirely solid. However, a similar effect can be obtained before the dendrites reached the center of the core if the liquid in the central region below the tip of the deepest dendrite is not being mixed with the inter-dendritic liquid (Haack and Scott, 1992). This is possible since the interdendritic liquid is richer in S and P and thus lighter than the liquid below the tip of the dendrites. We have therefore included the effects of assimilation in one of our IVA models of fractional crystallization.

Malvin (1988) suggested that the amount of liquid leaking into the core in each crystallization step was fixed. We find this unlikely since it becomes increasingly difficult to extract liquid metal from the mantle as it cools. Also, in our scenario it becomes increasingly difficult to find a source of pristine liquid as the dendrites penetrate to the center of the core and boundary layer liquid is contaminating the original liquid at all depths. We therefore chose to model assimilation by adding an amount of pristine liquid, in each crystallization step, which was proportional to the amount of liquid remaining in the core. In our model D we added an amount of liquid equal to 1% of the remaining liquid in each of the $10^4$ steps. The total amount of liquid thus added is 50 times the starting volume of liquid. This is equivalent to initially having only the upper 2 vol% of the liquid core taking part in the fractional crystallization. In this scenario the upper interdendritic liquid would be mixed by convection forced by the density differences due to S gradients. Thermal convection would probably continue in the lower part of the core although the release of latent heat in the upper core would make convection less vigorous. We do not consider this assimilation model (model D) to be realistic, but it is an extreme case that illustrates the effects of assimilation. In model D, we used the $K_S$ vs. S values from model C (Fig. 8).

#### 4.1.2. *Results of crystallization modeling*

Figure 9 shows the calculated fractional crystallization paths for group IVA from models A–D on Ni-Ge and Ni-

Table 5. Initial and final liquid compositions in our models of the fractional crystallization of the IVA core.

| | Au μg/g | Co mg/g | Ga μg/g | Ge μg/g | Ir μg/g | Ni wt% | S wt% | P wt% | Eutec. liquid vol% |
|---|---|---|---|---|---|---|---|---|---|
| Model A | | | | | | | | | |
| Initial | - | - | - | 0.115 | 2.0 | 8.40 | 2.5 | 0.25 | |
| Final | - | - | - | 0.000 | 0.00 | 9.68 | 27.5 | 1.65 | 8.9 |
| Model B | | | | | | | | | |
| Initial | - | - | - | 0.114 | 4.3 | 8.17 | 3.9 | 0.2 | |
| Final | - | - | - | 0.000 | 0.000 | 12.75 | 12.86 | 6.33 | 1.7 |
| Model C | | | | | | | | | |
| Initial | 1.50 | 3.95 | 2.0 | 0.115 | 2.0 | 8.40 | 2.5 | 0.25 | |
| Final | 4.81 | 5.01 | 0.001 | 0.000 | 0.000 | 12.76 | 12.86 | 6.33 | 2.2 |
| Model D | | | | | | | | | |
| Initial | 1.50 | 3.95 | 2.0 | 0.115 | 2.0 | 8.40 | 2.5 | 0.25 | |
| Final | 7.14 | 5.21 | 0.27 | 0.02 | 0.02 | 12.36 | 11.17 | 6.98 | - |

Ir plots. These plots, together with Ni-Ga were found by Haack and Scott (1993) to be the most sensitive to the choice of $K_S$, initial S, and the dependence of $K_S$ on S. We find that the IVA trends cannot be modeled with a model with $K_S = 0.01$ (model A), in which virtually all of the S is concentrated into the liquid. In particular the Ga and Ge trends in IVA, as in IIIAB (Haack and Scott, 1993), cannot be matched with such a model (Fig. 9a). The poor match is caused by the rapid increase in $K_{Ge}$ and $K_{Ga}$ with S. Although these distribution coefficients are larger than unity in IVA and the liquid is therefore being depleted in these elements, the solid concentration continues to increase due to the even faster increase in the distribution coefficients. Model B, which provides a slower increase in the S concentration following Haack and Scott (1993), therefore provides a better match to the relatively shallow Ga and Ge trends at high-Ni concentrations. In contrast, the low-Ni trends, which represent the initial part of the crystallization where the liquid S is still low, were not matched as well with model B. The shallow Ni-Ir trend and the steep Ni-Ga and Ni-Ge trends at low-Ni concentration are better modeled with model A ($K_S = 0.01$) for S concentrations less than 6 wt%. Model C satisfactorily combines the virtues of both models. (Note that only for model A was the initial liquid composition adjusted to maximize the match with the meteorite data. Liquid compositions for model B were chosen so that models B and C overlapped for liquids with >6% S)

Figure 10 shows the calculated crystallization trends from models C (our preferred closed-system model) and D (model C plus assimilation) for the other elements for which

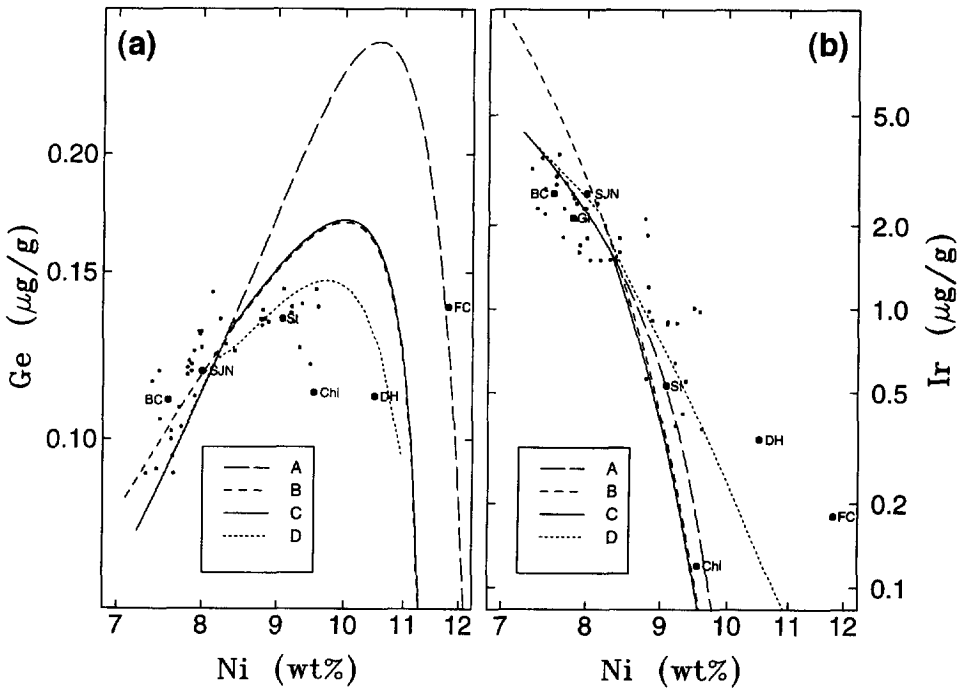


FIG. 9. Logarithmic plots showing comparisons of calculated solid compositions for models A–D with IVA data for (a) Ge against Ni and (b) Ir against Ni. Models A–C use the $K_S$-S relationships shown in Fig. 8. Model D uses the model C relationship with assimilation of primitive liquid throughout the crystallization of the core. Models C and D give the best matches to the IVA data.

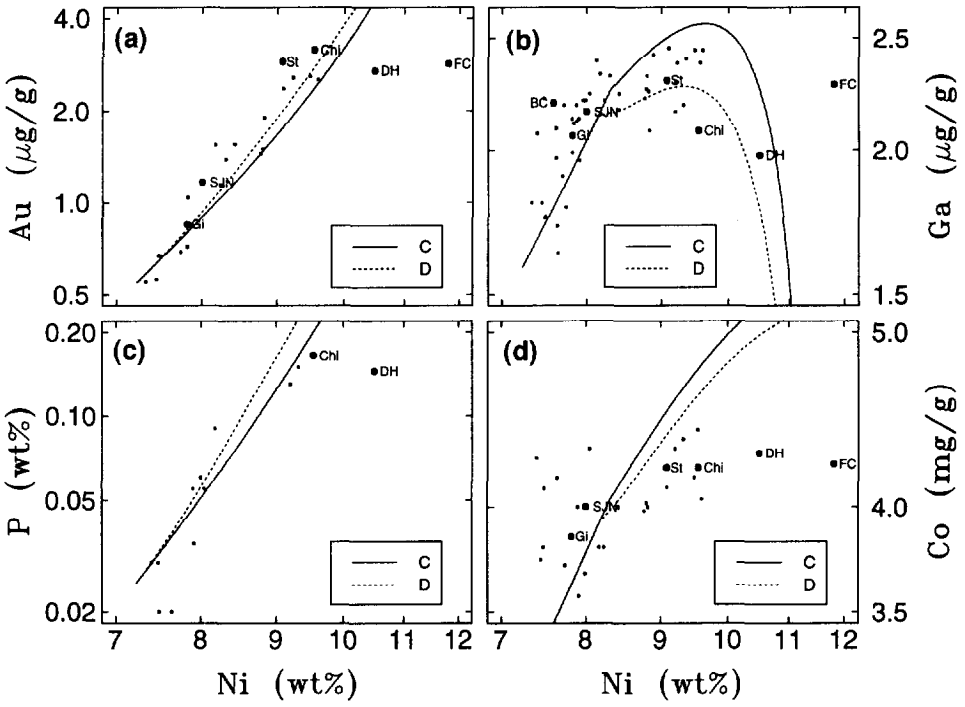


FIG. 10. Logarithmic plots showing comparisons of solid compositions calculated for fractional crystallization models C and D with IVA data for (a) Au, (b) Ga, (c) P, and (d) Co against Ni. At low-Ni concentrations the two models converge and match the IVA data adequately. At high-Ni concentrations, neither model matches the IVA trends.

distribution coefficients are available, Au, Ga, P, and Co (Jones and Malvin, 1990; Haack and Scott, 1993). Initial and final liquid compositions for models A–D are given in Table 5. Model C provides a good match to the IVA data up to ≈10 wt% Ni. At higher Ni concentrations, the IVA trends seem to level off for the elements Au, P, and Co. None of our models show this effect. However, the assimilation model (D) shows some improvement over the other models at high Ni concentrations for Ir (Fig. 9b). For low-Ni concentrations, where the compositions of the primitive and fractionally crystallizing liquids are similar, the differences between models C and D are insignificant. Although it seems unlikely that the original volume taking part in the fractional crystallization process was only 2% of the total core volume, as in model D, some kind of liquid mixing model may account for the poor match at high-Ni concentrations.

We have tested a range of models with different initial S concentration and find that the best match to the data is obtained with models having an initial S between 1.5 and 3.5 wt% S. Models with the higher initial S fit the Ni-Ge trend better, whereas models with the lower value fit the Ni-Ir trend better. Figure 11 shows the effect on model C of varying the initial S concentration between 1.5 and 3.5 wt% S. We choose 2.5 ± 1 wt% S as our best estimate of the initial S concentration. Figure 12a,b shows the variations of Ni in the crystallizing solid with the fraction crystallized and the S concentration in the liquid for the different models. Model C might be improved with a more gradual increase in the apparent distribution coefficient for S, but the overall match between model and data is not good enough to justify further modeling. Nevertheless, the match does imply that $K_S$ was much lower during the early part of the crystallization when the S concentration of the liquid was low.

The large scatter in compositions observed among the high-Ni irons, Chinautla, Duel Hill, and Fuzzy Creek, is consistent with the tendency in group IIIAB for the scatter to increase with increasing Ni concentration (Haack and Scott, 1993). During the final stages of core crystallization, km-sized dendrites may have inhibited core-wide mixing of the remaining liquid and there were probably wide variations in liquid mixing efficiency within and between the various reservoirs (Haack and Scott, 1993). However, it is difficult to explain the high Ni concentration of EET 83230 (16 wt%) on the basis of IVA fractional crystallization models. The highest Ni concentrations obtained with our numerical models are in the range 11–13 wt% Ni. Furthermore, our models predict very low solid concentrations of elements like Ir, Ga, and Ge in the highest Ni members of IVA. Although concentrations of these elements in EET 83230 are lower than in group IVA members with 7–12% Ni, the scatter and poor match for irons with >10% Ni prevent us from confidently classifying this iron as a IVA member.

Arguments like those used for IIIAB (Haack and Scott, 1993) suggest that our sample is broadly representative of the chemical diversity of solids that formed from the IVA magma, neglecting the small volume of S-rich material that represents the final stage of crystallization (Fig. 12). How-

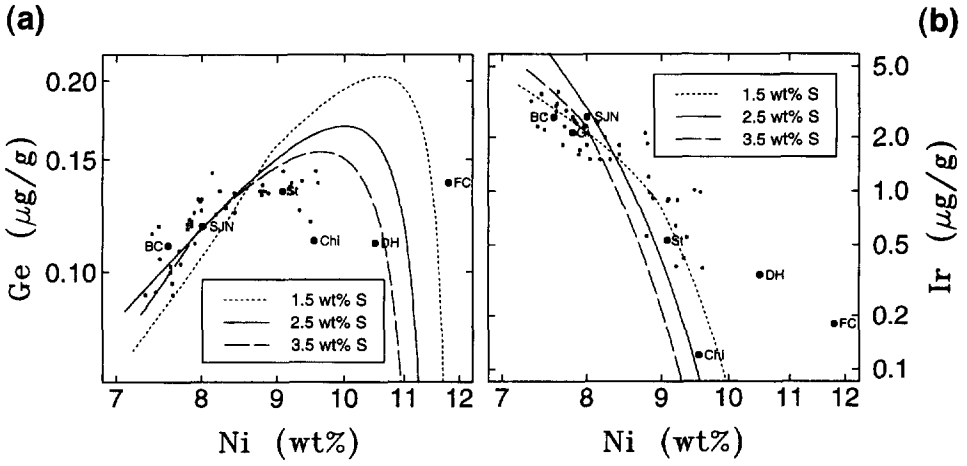


FIG. 11. Logarithmic plots of (a) Ge and (b) Ir against Ni for model C showing the effect of changing the initial S concentration in the liquid. A concentration of 2.5 wt% S gives the best overall match with IVA data: this is the value used in models A, C, and D in Figs. 9–10 and 12.

ever, the paucity of IVA members with 8.6 ± 0.2% Ni and discontinuities at this Ni concentration in kamacite bandwidth (Schaudy et al., 1972) and cooling rate (Rasmussen, 1982; Rasmussen et al., 1995) suggest that the high-Ni and low-Ni IVA irons may have been derived from separate regions in the IVA reservoir. The chemical trends in Figs. 1 and 2 do not show any strong evidence for a discontinuity around 8.6% Ni, but some of the difficulty in modeling IVA trends may arise because the IVA irons come from two or more dendrites that did not form in a single well-mixed magma.

Our fractional crystallization modeling suggests that the compositions of the metal fractions of São João Nepomuceno and Steinbach match the calculated solid compositions after 50% and 80%, respectively, of the magma fractionally crystallized (Fig. 12a). J. T. Wasson's value of 10.1% Ni for Steinbach (pers. commun., 1995) would increase this figure to 90%. Because of the scatter of analytical data, we cannot preclude the possibility that major amounts of liquid were trapped in the stony irons during crystallization of metallic liquid between silicates. Concentrations of troilite in the metallic portions of Steinbach and São João Nepomuceno (10–20 vol%; Tables 2, 4) are very much higher than any IVA iron (~3 vol%; Buchwald, 1975), indicating substantial trapping of liquid by silicates. Our models (Fig. 12) and the binary Fe-S phase diagram imply that the metal portion of the stony irons began to crystallize around 1400°C. This is below the temperature of the silica-pyroxene eutectic in the olivine–$SiO_2$ system for the Fe/(Fe + Mg) ratio of IVA stony irons, that is to say, about 1500°C (Morse, 1980). Silica-pyroxene mixtures could crystallize hundreds of degrees lower from a plagioclase-enriched liquid.

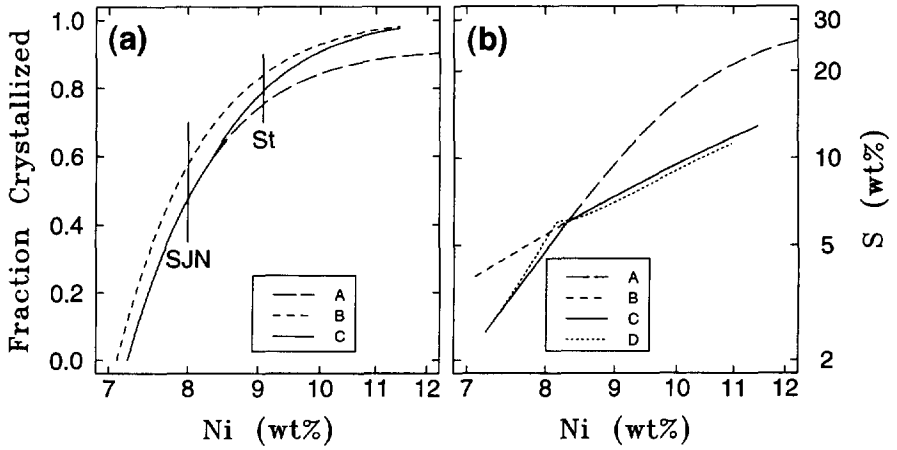


FIG. 12. Plots of (a) fraction of liquid crystallized and (b) S concentration in the liquid against the Ni concentration in the solid for the fractional crystallization models A–D plotted in Figs. 8–11. Metal compositions in the two IVA stony irons, São João Nepomuceno (SJN) and Steinbach (St), match the calculated solid composition after 50 ± 10% and 80 ± 10%, respectively, of the IVA core has fractionally crystallized. (Model D is omitted in (a) as primitive liquid is added during crystallization.)

### 4.2. Physical Setting for Crystallization

Rasmussen (1982) suggested that group IVA irons formed in two separate bodies in an attempt to explain the high and variable cooling rates of the low-Ni IVA irons and the rather uniform, low rates of the high-Ni irons. Cosmic-ray exposure age data do not exclude such a possibility. Although seven out of eight low-Ni IVA irons have exposure ages within error of 400 My indicating that they experienced a common exposure event, only one of the two high-Ni irons has this age (Voshage and Feldmann, 1979). However, the continuity of the chemical trends in low-Ni and high-Ni IVA irons and the paucity of ungrouped irons in Fig. 2 make it very likely that all the IVA irons and stony irons crystallized from a single reservoir. We show above that the IVA chemical trends can be modeled as well as those in group IIIAB by using a lower initial S concentration of 2.5 ± 1%. We therefore argue that IVA, like IIIAB, fractionally crystallized from a single reservoir.

If group IVA had crystallized from a small molten pool, we should expect to find some IVA irons containing wall-rock silicates with a mineralogy compatible with partial melting of chondritic material. But we do not. Instead, the abundance of IVA irons and the homogeneity of the numerous large Gibeon specimens with a total weight of 21 tons (Buchwald, 1975) suggest that the source was large, at least 100 m in diameter in size. Metal pools this big, unless formed in an impact, quickly sink through silicate (Taylor, 1992). An impact origin for molten IVA metal is very unlikely as impact melts on asteroids should contain abundant cool clasts and cool rapidly. We therefore conclude that the metal in IVA irons and stony irons was derived from a single molten core that fractionally crystallized.

### 4.3. Depletion of Moderately Volatile Siderophiles in IVA

An important difference between group IVA and most other groups like IIIAB is the large depletion of Ga, Ge, and Cu relative to Ni, when normalized to CI chondrites. Depletions of moderately volatile siderophile elements are more extensive in group IVB irons and some ungrouped irons than in group IVA. In all cases, the depletions are inversely correlated with nebular condensation temperature (Wai and Wasson, 1979). Moderately volatile siderophiles in irons show trends that are analogous to those of chondrites, except that the depletions in groups IVA and IVB are as much as 100–1000 times larger than those shown by any chondrite group (Palme et al., 1988). For example, Ga/Ni and Ge/Ni ratios in group IVA and IVB are $10^{-2}$–$10^{-4}$ times the CI chondrite values.

Certain chondrules are depleted in moderately volatile lithophiles much more than whole chondrites. Weisberg et al. (1990) found a Na/Mg ratio in Renazzo type I chondrules 0.03 times the CI value. Type II chondrules, which are much richer in volatiles, make up <1% of the chondrule population in Renazzo and other CR chondrites (Weisberg et al., 1993). Thus, it is possible that matrix-poor, CR-like chondrites will be found with much larger depletions than those in currently known chondrites, but by no means certain that their depletions will approach the values in IVA and IVB irons.

If the concentrations of moderately volatile elements in group IVA are not inherited from their chondritic precursors, some planetary mechanism must be invoked. Chalcophile elements may have been removed from differentiated asteroids by explosive loss of Fe–Ni–S melts, but Ga and Ge are siderophile and are depleted 1–100× more than S in group IVA and IVB irons (Keil and Wilson, 1993). Another planetary mechanism that might be invoked is impact. Wetherill (1992) has speculated that igneous meteorites may be fragments of lunar-sized planetary embryos that formed in the asteroid belt, whereas chondrites are from smaller planetesimals that failed to accrete into the lunar-sized bodies. It is unclear how large impacts, even of lunar-sized bodies, could fractionate volatile from refractory siderophiles. In addition, most iron meteorite groups have abundances of moderately volatile siderophiles that are comparable to those observed in chondrites. We conclude that planetary mechanisms are even less plausible than nebular ones for depleting moderately volatile siderophiles in group IVA and IVB irons.

Group IVB irons and similarly depleted ungrouped irons do not share any unusual characteristic with group IVA besides a low abundance of moderately volatile siderophiles. Group IVB irons, for example, have uniform cooling rates consistent with a core origin (Rasmussen, 1989) and do not contain silicates. (A tentative identification of silicates in the IVB iron, Weaver Mountains by Buchwald (1975) needs confirmation.) It therefore seems unlikely that there is any connection between the low volatile content of group IVA and its unusual silicates and wide range of metallographic cooling rates.

### 4.4. Origin of Silicates in IVA Irons and Stony-Irons

Prinz et al. (1984) briefly outlined two models for the formation of silicates in IVA stony irons; both models have major problems but other models have not been proposed. In the first model, a pallasite-like olivine cumulate is converted to low-Ca pyroxene and silica by reaction with Si-bearing metal. Prinz et al. (1984) preferred a two-stage model in which an olivine-pyroxene cumulate is first formed from a chondritic liquid. A second heating event after 'migration of incompatible elements' causes eutectic melting on the pyroxene–$SiO_2$ join. Neither model specifically addresses how metal and silicate were mixed. Here we will briefly discuss certain aspects of these models and propose an alternative model.

Occurrences of silica in the IVA irons, Gibeon and Bishop Canyon, may be unrelated to those in the stony irons in view of the differences in morphology and composition. Concentrations of Na and Al in silica in the two irons are much lower than in the stony irons (Table 3). Although trace amounts of silica have been reported in a few IIAB and IIIAB irons (Kracher et al., 1977; R. W. Bild, pers. commun. 1991), silica appears to be more abundant in the IVA irons than in other groups as the rare grains in Bishop Canyon and Gibeon are exceptionally large. The silica plates in the IVA irons may have formed during crystallization of the

Fe,Ni core in the same way that phosphates in troilite nodules in many irons are believed to have crystallized (Buchwald, 1984).

Prinz et al. (1984) suggested that the proportions of silica and pyroxene in the IVA stony irons are appropriate for a eutectic mixture. However, our data and those of Prinz et al. (1984) show that the pyroxene-tridymite ratio in Steinbach (1.9 and 1.3) is significantly lower than in São João Nepomuceno (7.4 and 5.5). Although our value for São João Nepomuceno is close to the eutectic value for the $SiO_2$–$MgSiO_3$ system, substitution of FeO would give a higher value (Morse, 1980). Averaging data for Steinbach and São João Nepomuceno, as Prinz et al. (1984) suggest, does not provide convincing support for an origin as a binary eutectic liquid.

In support of some pallasite-like origin for the IVA stony irons, there are certain similarities between the metal-silicate textures in the IVA stony irons and those in pallasites that have rounded olivines, like Brenham. These similarities include the rather uniform proportions of silicate and metal and the sizes of silicate grains. In rounded-olivine pallasites this texture is attributed to the weight of cumulate olivine crystals depressing olivine crystals into the denser metallic Fe,Ni at the core-mantle boundary (Wood, 1981). An analogous phenomenon is observed in nickel sulfide deposits at the base of ultramafic flows (Usselman et al., 1979). Brenham and São João Nepomuceno also contain large silicate-free volumes of metal that separate uniform metal-silicate volumes. This is best illustrated by comparing the IVA stony iron to the slice of the Brenham pallasite shown in Plate XVII of Nininger (1952). These silicate-free zones may result from late impact or tectonic events.

In theory, olivine in a pallasitic assemblage could be converted to pyroxene-silica in a Steinbach-like assemblage by reducing fayalite to metal and silica using Si in metallic Fe,Ni. Low-Ca pyroxene could form by reacting silica with olivine. A more plausible precursor would be a pyroxene-bearing pallasite, like Yamato 8451 (Yanai and Kojima, 1995), as the IVA pyroxenes contain significant amounts of Ca and Al that could not be obtained from a pure-olivine source. However, it is very difficult to derive enough Si from the metal core as the IVA pyroxenes are currently much more oxidized (Fs 14-15) than those in equilibrium with Si-rich metal, such as in equilibrated E chondrites. In the IVA core we should expect only ppm levels of Si when it was molten (e.g., Wasson et al., 1994). Even if this Si reacted with FeO-bearing olivines on cooling, the volume of any Steinbach-like products would be trivial. Crystallization of silica-pyroxene from a silica-rich magma is more plausible (Ulff-Møller et al., 1995).

Since static models of slowly cooling asteroids do not provide plausible environments for the mixing core metal with $SiO_2$-rich silicates, we briefly consider a dynamic model. Haack et al. (1995) find from their transmission electron microscopic studies of the Steinbach pyroxenes that they were quenched from 1200°C in a few hours, confirming the work of Reid et al. (1974). Haack et al. (1995) conclude from this and other thermal constraints that the IVA parent body was impacted by a large projectile after the core had largely crystallized and that fragments of core and mantle were mixed together and reaccreted. If this event mixed hot metal fragments and S-rich metallic liquids with $SiO_2$-rich rocks, it may have generated a partial melt capable of crystallizing low-Ca pyroxene and silica simultaneously. Residual plagioclase-rich liquid could have been removed when these silicates were depressed into molten S-rich metal.

The large size of the silica and pyroxene crystals in the IVA stony irons may not be incompatible with the rapid subsolidus cooling rates indicated by Haack et al. (1995) as some chondrules have formed large crystals of these phases. However, the small compositional differences between orthopyroxene and clinopyroxene (Table 3) require some subsolidus equilibration. Detailed thermal models are required to test this model further.

*Acknowledgments*—We thank R. S. Clarke Jr., C. B. Moore, J. T. Wasson, K. L. Rasmussen, and H.-J. Blankenburg for the kind loan of samples, and F. Ulff-Møller, K. L. Rasmussen, G. J. Taylor, and J. I. Goldstein for helpful discussions and for sharing unpublished data. K. Horton, T. Hulsebosch, T. Servilla, and T. Tatnall are thanked for expert technical assistance, and G. Gina Ling for her help with Chinese translations. J. T. Wasson, K. L. Rasmussen, R. W. Bild, and A. H. Treiman kindly provided helpful reviews. This work was partly supported by NASA grant NAGW 3281 to K. Keil. This is Hawai'i Institute of Geophysics and Planetology publication no. 871 and School of Ocean and Earth Science and Technology publication no. 4058.

*Editorial handling:* H. E. Newsom

## REFERENCES

Bian D. (1981) Chinese meteorites. *Meteoritics* **16,** 115–127.

Bild R. W. (1976) A study of primitive and unusual meteorites. Ph.D. thesis, Univ. California, Los Angeles.

Bild R. W. (1977) Compositions of silicate inclusions as an aid in the classification of iron meteorites and a tentative classification of Britstown. *Meteoritics* **12,** 177 (abstr.).

Buchwald V. F. (1975) *Handbook of Iron Meteorites.* Univ. California Press.

Buchwald V. F. (1984) Phosphate minerals in meteorites and lunar rocks. In *Phosphate Minerals* (ed. J. O. Nriagu and P. B. Moore), pp. 199–214. Springer-Verlag.

Choi B.-G., Ouyang X., and Wasson J. T. (1995) Classification and origin of IAB and IIICD iron meteorites. *Geochim. Cosmochim. Acta* **59,** 593–612.

Clayton R. N., Mayeda T. K., Olsen E. J., and Prinz M. (1983) Oxygen isotope relationships in iron meteorites. *Earth Planet. Sci. Lett.* **65,** 229–232.

Çolakoglu K. and Ceylan M. (1988) An iron meteorite from Akyumak. *Meteoritics* **23,** 371–372.

Creaser R. A., Papanastassiou D. A., and Wasserburg G. J. (1993) Rhenium-Osmium isotope systematics of group IIA and group IVA iron meteorites. *Lunar Planet. Sci.* **XXIV,** 339–340 (abstr.).

Dollase W. A. (1967) The crystal structure at 220°C of orthorhombic high tridymite from the Steinbach meteorite. *Acta Cryst.* **23,** 617–623.

Fouché K. F. and Smales A. A. (1966) The distribution of gold and rhenium in iron meteorites. *Chem. Geol.* **1,** 329–339.

Graham A. L., Bevan A. W. R., and Hutchison R. (1985) *Catalogue of Meteorites,* 4th Ed. British Museum (Natural History).

Haack H. and Scott E. R. D. (1992) Asteroid core crystallization by inward dendritic growth. *J. Geophys. Res.* **97,** 14727–14734.

Haack H. and Scott E. R. D. (1993) Chemical fractionations in group IIIAB iron meteorites: Origin by dendritic crystallization of an asteroidal core. *Geochim. Cosmochim. Acta* **57,** 3457–3472.

Haack H., Scott E. R. D., Love S. G., Brearley A. J., and McCoy T.

J. (1995) Thermal histories of IVA stony-iron and iron meteorites: evidence for asteroid fragmentation and reaccretion. *Geochim. Cosmochim. Acta* (submitted).

Hoashi M., Varela-Alvarez H., Brooks R. R., Reeves R. D., Ryan D. E., and Holzbecher J. (1992) Revised classification of some iron meteorites by use of statistical procedures. *Chem. Geol.* **98,** 1–10.

Hoppe G. (1975) Gesamtkatalog der in der Deutschen Demokratischen Republik vorhandenen Meteorite. Wissen. Zeit. Humboldt-Univ. Berlin, Math.-Nat. R. **XXIV,** 521–533.

Jarosewich E. (1990) Chemical analysis of meteorites: A compilation of stony and iron meteorite analyses. *Meteoritics* **25,** 323–337.

Jones J. H. and Drake M. J. (1983) Experimental investigations of trace element fractionation in iron meteorites. II: The influence of sulfur. *Geochim. Cosmochim. Acta* **47,** 1199–1209.

Jones J. H. and Malvin D. J. (1990) A nonmetal interaction model for the segregation of trace elements during solidification of Fe–Ni–S, Fe–Ni–P, and Fe–Ni–S–P alloys. *Metall. Trans. B* **21B,** 697–706.

Keil K. and Wilson L. (1993) Explosive volcanism and the compositions of cores of differentiated asteroids. *Earth Planet. Sci. Lett.* **117,** 111–124.

Kracher A., Kurat G., and Buchwald V. F. (1977) Cape York: The extraordinary mineralogy of an ordinary iron meteorite and its implications for the genesis of IIIAB irons. *Geochem. J.* **11,** 207–217.

Kracher A., Willis J., and Wasson J. T. (1980) Chemical classification of iron meteorites—IX. A new group (IIF), revision of IAB and IIICD, and data on 57 additional irons. *Geochim. Cosmochim. Acta* **44,** 773–787.

Lewis C. F. and Moore C. B. (1971) Chemical analyses of thirty-eight iron meteorites. *Meteoritics* **6,** 195–205.

Li Z., Liang Z., Zhou H., Li Y., Zhao D., and Zhang M. (1979) Spark source mass spectrometric analysis of some iron meteorites from China (in Chinese). *Geochimica,* 273–278.

Malvin D. J. (1988) Assimilation-fractional crystallization modelling of magmatic iron meteorites. *Lunar Planet. Sci.* **XIX,** 720–721 (abstr.).

Malvin D. J., Wang D., and Wasson J. T. (1984) Chemical classification of iron meteorites—X. Multielement studies of 43 irons, resolution of group IIIE from IIIAB, and evaluation of Cu as a taxonomic parameter. *Geochim. Cosmochim. Acta* **48,** 785–804.

McCall G. J. H. (1973) *Meteorites and Their Origins.* Wiley.

McCoy T. J., Keil K., Scott E. R. D., and Haack H. (1993) Genesis of IIICD iron meteorites: Evidence from silicate-bearing inclusions. *Meteoritics* **28,** 552–560.

Moore C. B., Lewis C. F., and Nava D. (1969) Superior analysis of iron meteorites. In *Meteorite Research* (ed. P. M. Millman), pp. 738–748.

Moren A. E. and Goldstein J. I. (1978) Cooling rate variations of group IVA iron meteorites. *Earth Planet. Sci. Lett.* **40,** 151–161.

Moren A. E. and Goldstein J. I. (1979) Cooling rates of group IVA iron meteorites determined from a ternary Fe–Ni–P model. *Earth Planet. Sci. Lett.* **43,** 182–196.

Morse S. A. (1980) *Basalts and Phase Diagrams.* Springer-Verlag.

Nininger H. H. (1952) *Out of the Sky.* Dover.

Palme H., Larimer J. W., and Lipschutz M. E. (1988) Moderately volatile elements. In *Meteorites and the Early Solar System* (ed. J. F. Kerridge and M. S. Matthews), pp. 436–461. Univ. Arizona Press.

Pernicka E. and Wasson J. T. (1987) Ru, Re, Os, Pt, and Au in iron meteorites. *Geochim. Cosmochim. Acta* **51,** 1717–1726.

Prinz M., Nehru C. E., Delaney J. S., Fredriksson K., and Palme H. (1984) Silicate inclusions in IVA iron meteorites. *Meteoritics* **19,** 291–292 (abstr.).

Rasmussen K. L. (1982) Determination of the cooling rates and nucleation histories of eight group IVA iron meteorites using local bulk Ni and P variation. *Icarus* **52,** 444–453.

Rasmussen K. L. (1989) Cooling rates and parent bodies of iron meteorites from groups IIICD, IAB and IVB. *Phys. Scripta* **39,** 410–416.

Rasmussen K. L., Ulff-Møller F., and Haack H. (1995) The thermal evolution of the IVA iron meteorites: Evidence from metallographic cooling rates. *Geochim. Cosmochim. Acta* **59,** 3049–3059.

Reid A. M., Williams R. J., and Takeda H. (1974) Coexisting bronzite and clinobronzite and the thermal evolution of the Steinbach meteorite. *Earth Planet. Sci. Lett.* **22,** 67–74.

Rösler H. J., Blankenburg H.-J., and Baum H. (1978) Neuere Untersuchungen am Meteoriten von Rittersgrün/Erzgebirge. *Chem. Erde* **37,** 242–264.

Ryan D. E., Holzbecher J., and Brooks R. R. (1990) Rhodium and osmium in iron meteorites. *Chem. Geol.* **85,** 295–303.

Schaudy R., Wasson J. T., and Buchwald V. F. (1972) The chemical classification of iron meteorites. VI. A reinvestigation of irons with Ge concentrations lower than 1 ppm. *Icarus* **17,** 174–192.

Scott E. R. D. (1972) Chemical fractionation in iron meteorites and its interpretation. *Geochim. Cosmochim. Acta* **36,** 1205–1236.

Scott E. R. D. (1978a) Tungsten in iron meteorites. *Earth Planet. Sci. Lett.* **39,** 363–370.

Scott E. R. D. (1978b) Iron meteorites with low Ga and Ge concentrations: Composition, structure and genetic relationships. *Geochim. Cosmochim. Acta* **42,** 1243–1251.

Scott E. R. D. and Wasson J. T. (1976) Chemical classification of iron meteorites—VIII. Groups IC, IIE, IIIF and 97 other irons. *Geochim. Cosmochim. Acta* **40,** 103–115.

Sellamuthu R. and Goldstein J. I. (1985) Analysis of segregation trends observed in iron meteorites using measured distribution coefficients. *Proc. 15th Lunar Planet. Sci. Conf.; J. Geophys. Res.* **90,** C677–C688.

Smales A. A., Mapper D., and Fouché K. F. (1967) The distribution of some trace elements in iron meteorites, as determined by neutron activation. *Geochim. Cosmochim. Acta* **31,** 673–720.

Taylor G. J. (1992) Core formation in asteroids. *J. Geophys. Res.* **97,** 14717–14726.

Taylor G. J., Maggiore P., Scott E. R. D., Rubin A. E., and Keil K. (1987) Original structures and fragmentation and reassembly histories of asteroids: evidence from meteorites. *Icarus* **69,** 1–13.

Ulff-Møller F., Rasmussen K. L., Prinz M., Palme H., Spettel B., and Kallemeyn G. W. (1995) Magmatic activity on the IVA parent body: Evidence from silicate-bearing iron meteorites. *Geochim. Cosmochim. Acta* **59,** 4713–4728.

Usselman T. M., Hodge D. S., Naldrett A. J., and Campbell I. H. (1979) Physical constraints on the characteristics of nickel-sulfide ore in ultramafic lavas. *Can. Mineral.* **17,** 361–372.

Voshage H. and Feldmann H. (1979) Investigations on cosmic-ray produced nuclides in iron meteorites, 3. Exposure ages, meteoroid sizes and sample depths determined by mass spectrometric analyses of potassium and rare gases. *Earth Planet. Sci. Lett.* **45,** 293–308.

Wai C. M. and Wasson J. T. (1979) Nebular condensation of Ga, Ge and Sb and the chemical classification of iron meteorites. *Nature* **282,** 790–793.

Wasson J. T. (1974) *Meteorites—Classification and Properties.* Springer-Verlag.

Wasson J. T. (1990) Ungrouped iron meteorites in Antarctica: origin of anomalously high abundance. *Science* **249,** 900–902.

Wasson J. T., Ouyang X., Wang J., and Jerde E. (1989) Chemical classification of iron meteorites-XI. Multi-element studies of 38 new irons, and the high abundance of ungrouped irons from Antarctica. *Geochim. Cosmochim. Acta* **53,** 735–744.

Wasson J. T., Kallemeyn G. W., and Rubin A. E. (1994) Equilibration temperatures of EL chondrites: A major downward revision of the ferrosilite contents of enstatite. *Meteoritics* **29,** 658–662.

Weisberg M. K., Prinz M., and Nehru C. E. (1990) The Bencubbin chondrite breccia and its relationship to CR chondrites and the ALH85085 chondrite. *Meteoritics* **25,** 269–279.

Weisberg M. K., Prinz M., Clayton R. N., and Mayeda T. K. (1993) The CR (Renazzo-type) carbonaceous chondrite group and its implications. *Geochim. Cosmochim. Acta* **57,** 1567–1586.

Wetherill G. W. (1992) An alternative model for the formation of the asteroids. *Icarus* **100,** 307–325.

Willis J. and Goldstein J. I. (1982) The effects of C, P, and S on trace element partitioning during solidification in Fe-Ni alloys.

*Proc. 13th Lunar Planet. Sci. Conf.; J. Geophys. Res.* **87,** A435–A445.

Willis J. and Wasson J. T. (1978a) Cooling rates of group IVA iron meteorites. *Earth Planet. Sci. Lett.* **40,** 141–150.

Willis J. and Wasson J. T. (1978b) A core origin for group IVA iron meteorites: A reply to Moren and Goldstein. *Earth Planet. Sci. Lett.* **40,** 162–167.

Wood J. A. (1981) On the nature of the pallasite parent body: midcourse corrections. *Lunar Planet. Sci.* **XII,** 1200–1202 (abstr.).

Yanai K. and Kojima H. (1995) Yamato-8451: A newly identified pyroxene-bearing pallasite. *Proc. Nat. Inst. Polar Res. (Tokyo) Symp. Antarctic Meteorites* **8,** 1–10.

## APPENDIX

Table A1 lists all the sources of data for IVA irons and stony irons that we have plotted in Figs. 1 and 2. The names of all IVA members and the references for their classification are given in Table A2.

Malvin et al. (1984) found that three of the five IVA irons from China have compositions that are virtually indistinguishable: Huangling, Guanghua, and Yingde. Although they can be distinguished from all other analyzed IVA irons, Malvin et al. (1984) tentatively concluded that the three were not paired. We have italicized all three irons in Table A2, as we believe it is likely that the three samples analyzed by Malvin et al. (1984) come from a single meteorite.

Malvin et al. (1984) suggested that Huangling might resemble Steinbach and São João Nepomuceno because Bian (1981) had tentatively listed it as a mesosiderite. However, this classification by Bian (1981) was not based on petrographic study but on the analysis of the metal by Li et al. (1979), who did not identify any mineralogical features characteristic of mesosiderites. The large discrepancy between the analyses of Li et al. (1979) and Malvin et al. (1984) raises the possibility that their samples were from different meteorites. Since Malvin et al. (1984) analyzed only drillings of Huangling, it is possible that their sample was a mislabeled specimen of Guanghua, which was found in the same province.

Malvin et al. (1984) argued that it was unlikely that Guanghua and Yingde were related because the 300 kg Yingde was found 1000 km to the south of Guanghua. However, the history of Yingde is poorly known: it was recovered in either 1860 or 1964 (Bian, 1981). We therefore consider it more plausible that these two meteorites are paired. In Figs. 1 and 2 and 9–11 we have plotted only the mean values of the analytical data for Huangling, Guanghua, and Yingde obtained by Malvin et al. (1984).

All data for Longchang (IVA-An) were omitted as Malvin et al. (1984) believed it had been contaminated when forged. In addition, the Ge analysis of Novorybinskoe by Scott and Wasson (1976) was excluded as contamination problems clearly affected the analysis.

Table A1. Sources of analytical data for IVA irons.

| Source | As | Au | Co | Ga | Ge | P | Ir | Ni | Re | W | No. irons |
|---|---|---|---|---|---|---|---|---|---|---|---|
| Creaser et al. (1993) | | | | | | | | | x | | 5 |
| Fouché and Smales (1966) | | x | | | | | | | x | | 4 |
| Hoashi et al. (1992) | x | x | | | | | x | | | | 1 |
| Jarosewich (1990) * | | | x | | | x | | x | | | 3 |
| Kracher et al. (1980) † | | | | x | x | | x | x | | | 5 |
| Lewis and Moore (1971) | | | x | | | x | | | | | 2 |
| Malvin et al. (1984) § | x | x | x | x | x | | x | x | x | x | 8 |
| Moore et al. (1969) | | | x | | | x | | | | | 12 |
| Ryan et al. (1990) | x | x | | | | | | | | | 6 |
| Schaudy et al. (1972) | | | | x | x | | x | x | | | 36 |
| Scott (1978a) | | | | | | | | | | x | 6 |
| Scott and Wasson (1976) | | | | x | x | | x | x | | | 3 |
| Smales et al. (1967) | x | x | | | | | | x | | | 11 |
| This work | x | x | x | | | | x | | x | | 6 |
| Wasson et al. (1989) | x | x | x | x | x | | x | x | x | x | 3 |

* ALH A77255 is ungrouped, not a IVA iron (Malvin et al., 1984).
† See also Table 7.
§ See also Table 3.

Table A2. Meteorites belonging to group IVA*.

Akyumak[a], Allan Hills A78252[b], Altonah, Alvord[e], Bishop Canyon, Bodaibo, Boogaldi, Bristol, Bushman Land, Charlotte, Chinautla, Cleburne[e], Cranberry Plains[e], Cratheus (1931), Duchesne, Duel Hill (1854)[d], Elephant Moraine 83230 (?)[g], Fuzzy Creek[d], Gibeon[c], *Guanghua*[d†], Harriman (Of), Hill City, *Huangling*[d†], Huizopa, Iron River, Jamestown, La Grange, Longchang[d], Mantos Blancos, Maria Elena (1935), Mart, Millarville[c], Mt. Sir Charles[c], Muonionalusta, New Westville, Ningbo[d], Novorybinskoe[b], Obernkirchen, Otchinjau, Para de Minas, Putnam County, Rembang[b], Rica Aventura[c], San Francisco Mtns., São João Nepomuceno[c], Seneca Township, Serrania de Varas, Shirahagi[b], Signal Mountain, Smithland, Social Circle, Steinbach, Western Arkansas, Wood's Mountain, Yanhuitlan, *Yingde*[d†], Yudoma[f].

* Classifications are from Schaudy et al. (1972) except as noted: a) Çolakoglu and Ceylan (1988); b) Scott and Wasson (1976); c) Kracher et al., (1980); d) Malvin et al., (1984); e) Wasson et al., (1989); f) Buchwald (1975) and Graham et al. (1985), g) this work. Omitted from this list is Railway (Schaudy et al., 1972), also known as South African Railways (Graham et al., 1985), as it is paired with Gibeon, according to Buchwald (1975).

† These three irons are italicized because we believe that Guanghua and Yingde are paired, and the sample of Huangling analyzed by Malvin et al. (1984) may have been mislabelled.